SMC-TR-04-07

AEROSPACE REPORT NO.
TR-2004(8555)-2

Continuous-Wave Tunable Midwave Infrared Generation Near 4.5 μm with an Intracavity Optical Parametric Oscillator and Difference Frequency Generation

30 December 2003

Prepared by

D.-W. CHEN
Electronics and Photonics Laboratory
Laboratory Operations

Prepared for

SPACE AND MISSILE SYSTEMS CENTER
AIR FORCE SPACE COMMAND
2430 E. El Segundo Boulevard
Los Angeles Air Force Base, CA 90245

Engineering and Technology Group

THE AEROSPACE CORPORATION
El Segundo, California

This report was submitted by The Aerospace Corporation, El Segundo, CA 90245-4691, under C
tract No. FA8802-04-C-0001 with the Space and Missile Systems Center, 2430 E. El Segundo B
Los Angeles Air Force Base, CA 90245. It was reviewed and approved for The Aerospace Corp
tion by B. Jaduszliwer, Principal Director, Electronics and Phtonics Laboratory. Michael Zambr
was the project officer for the Mission-Oriented Investigation and Experimentation (MOIE) prog

This report has been reviewed by the Public Affairs Office (PAS) and is releasable to the Nation
Technical Information Service (NTIS). At NTIS, it will be available to the general public, inclu
foreign nationals.

This technical report has been reviewed and is approved for publication. Publication of this repo
does not constitute Air Force approval of the report's findings or conclusions. It is published onl
the exchange and stimulation of ideas.

Michael Zambrana
SMC/AXE

REPORT DOCUMENTATION PAGE

Form Approved
OMB No. 0704-0188

1. REPORT DATE (*DD-MM-YYYY*)	2. REPORT TYPE	3. DATES COVERED (*From - To*)
30-12-2003		

4. TITLE AND SUBTITLE

Continuous-Wave Tunable Midwave Infrared Generation Near 4.5 μm with an Intracavity Optical Parametric Oscillator and Difference Frequency Generation

5a. CONTRACT NUMBER
FA8802-04-C-0001

5b. GRANT NUMBER

5c. PROGRAM ELEMENT NUMBER

6. AUTHOR(S)

D.-W. Chen

5d. PROJECT NUMBER

5e. TASK NUMBER

5f. WORK UNIT NUMBER

7. PERFORMING ORGANIZATION NAME(S) AND ADDRESS(ES)

The Aerospace Corporation
Laboratory Operations
El Segundo, CA 90245-4691

8. PERFORMING ORGANIZATION REPORT NUMBER

TR-2004(8555)-2

9. SPONSORING / MONITORING AGENCY NAME(S) AND ADDRESS(ES)

Space and Missile Systems Center
Air Force Space Command
2450 E. El Segundo Blvd.
Los Angeles Air Force Base, CA 90245

10. SPONSOR/MONITOR'S ACRONYM(S)
SMC

11. SPONSOR/MONITOR'S REPORT NUMBER(S)
SMC-TR-04-07

12. DISTRIBUTION/AVAILABILITY STATEMENT

Approved for public release; distribution unlimited.

13. SUPPLEMENTARY NOTES

14. ABSTRACT

Continuously tunable cw emission near 4.5 μm was generated by difference frequency generation (DFG) within a Nd:YAG pumped optical parametric oscillator (OPO). The periodically poled lithium niobate crystal used for DFG contained eight grating bands that enabled wavelength tuning between 4.25 and 5.65 μm. As much as 90 mW of power at 4.48μm was achieved for 16.7 W of pump.

15. SUBJECT TERMS
Difference frequency generaton, Nd:YAG, Optical parametric oscillator, Lithium niobate

16. SECURITY CLASSIFICATION OF:			17. LIMITATION OF ABSTRACT	18. NUMBER OF PAGES	19a. NAME OF RESPONSIBLE PERSON
a. REPORT	b. ABSTRACT	c. THIS PAGE		5	Da-Wun Chen
UNCLASSIFIED	UNCLASSIFIED	UNCLASSIFIED			19b. TELEPHONE NUMBER (*include area code*) (310)336-7952

Note

The material reproduced in this report originally appeared in *Journal of the Optical Society of America B*. The TR is published to document the work for the corporate record.

Continuous-wave tunable midwave infrared generation near 4.5 μm with an intracavity optical parametric oscillator and difference frequency generation

Da-Wun Chen

Photonics Technology Department, Electronics and Photonics Laboratory, The Aerospace Corporation, 2350 East El Segundo Boulevard, El Segundo, California 90245

Received September 27, 2002; revised manuscript received February 3, 2003

Continuously tunable cw emission near 4.5 μm was generated by difference frequency generation (DFG) within a Nd:YAG pumped optical parametric oscillator (OPO). The periodically poled lithium niobate crystal used for DFG contained eight grating bands that enabled wavelength tuning between 4.25 and 4.65 μm. As much as 90 mW of power at 4.48 μm was achieved for 16.7 W of pump. © 2003 Optical Society of America

OCIS codes: 140.3070, 140.3600, 140.3580, 190.2620, 190.4970, 190.4360.

1. INTRODUCTION

Tunable, high-power, cw sources in the midwave infrared (MWIR) 4–5-μm region are desirable for many applications, such as spectroscopy and atmospheric and environmental sensing. Optical parametric oscillators (OPOs) that use periodically poled lithium niobate (PPLN) have exhibited both high conversion efficiency and a wide tuning range for cw operation in the infrared region up to 4 μm.[1,2] Beyond 4 μm, however, the OPO process in PPLN becomes inefficient because of the absorption of the mid-IR output.[3,4] In previous research, very low power (<1 mW) was reported slightly beyond 4 μm for a cw OPO[5] and difference frequency generation (DFG)[6] in PPLN. For pulsed OPOs, however, output wavelengths as great as 6.8 μm have been achieved with PPLN by use of ultrashort pump pulses (high peak power) and a very short (1-mm) crystal to minimize absorption.[7] Recently, Chen and Masters generated 150 mW of cw power at 4.3 μm by using a resonant cavity and a single PPLN crystal for both an OPO and DFG.[8] This simple configuration solved the high threshold problem but prevented tunability because of the unique phase-matching conditions that had to be met for the OPO and the DFG processes to occur within the same PPLN crystal at a single temperature. To achieve tunable output, two separate PPLN crystals were used within the resonator to allow for independent temperature phase matching of the two nonlinear processes. This two-crystal approach, although more difficult to align, yields the ability to optimize each of the nonlinear conversion processes independently for wavelength tuning.

2. THEORETICAL DESCRIPTION

The theory of quasi-phase-matched OPOs is well described in Ref. 9. The wave vector mismatch Δk_Q for the first-order quasi-phase-matched collinear process is

$$\Delta k_Q = k_p - k_s - k_i - 2\pi/\Lambda, \tag{1}$$

where k_p, k_s, k_i, and Λ are the wave vectors of the pump, the signal, the idler, and the PPLN grating period, respectively. The wave vector has magnitude $k = 2\pi n/\lambda$, where n is the refractive index and λ is the wavelength. The operating point of a quasi-phase-matched OPO is determined by the simultaneous solution of the energy conservation and momentum conservation (phase matching $\Delta k_Q = 0$) conditions, so that

$$1/\lambda_p = 1/\lambda_s + 1/\lambda_i, \tag{2}$$

$$n_p/\lambda_p = n_s/\lambda_s + n_i/\lambda_i + 1/\Lambda_1. \tag{3}$$

For a given OPO PPLN period Λ_1, pumping wavelength, and crystal temperature, OPO signal and idler wavelengths can be derived from Eqs. (2) and (3) and the Sellmeier equation for the refractive index. Alternatively, the required PPLN period Λ_1 can be calculated to achieve the desired OPO wavelengths for a given pump wavelength and temperature.

In this study, an OPO was pumped by a Nd:YAG laser at 1.06 μm. The OPO signal and idler waves were subsequently used to generate the MWIR wavelength through the DFG process. All three waves satisfy energy and momentum conservation conditions analogous to those in Eqs. (2) and (3), so that

$$1/\lambda_{\mathrm{MWIR}} = 1/\lambda_s - 1/\lambda_i, \tag{4}$$

$$n_{\mathrm{MWIR}}/\lambda_{\mathrm{MWIR}} = n_s/\lambda_s - n_i/\lambda_i - 1/\Lambda_2. \tag{5}$$

For a selected DFG PPLN grating Λ_2 and temperature, we obtained the pair of OPO signal and idler waves that satisfy Eqs. (4) and (5) by temperature tuning the OPO PPLN crystal.

0740-3224/2003/071527-05$15.00

3. EXPERIMENTAL SETUP

A. Optical Parametric Oscillator and Difference Frequency Generation Resonant Cavity

The revised OPO and DFG ring cavity from Ref. 8 and illustrated in Fig. 1 was constructed with four 10-cm radii of curvature mirrors. All four mirrors were coated for high reflectivity ($R > 99.8\%$) to resonate the OPO signal wavelengths in the 1.65–1.75-μm range. In addition, the input coupler M_1 was coated for high transmission ($T > 98\%$) at the pump wavelength of 1.06 μm, M_2 and M_3 were HR coated ($R > 99\%$) for OPO idler wavelengths of 2.7–3.0 μm, and CaF_2 output coupler M_4 was HT coated ($T > 85\%$) for the DFG output at 4–5 μm. A 4-μm-long-pass filter F was used for DFG output power measurement. The OPO and DFG crystals were placed between M_1 and M_2 and M_3 and M_4, respectively. The M_1 to M_2 and M_3 to M_4 mirror spacings were 20.5 cm, whereas the remaining mirror separations were 21.5 cm. This four-mirror configuration forms a symmetric and stable ring cavity with two identical 90-μm mode waists (radius) for the resonant OPO signal wavelength at the center of each crystal. The resonant cavity was pumped by an arc-lamp-pumped cw Nd:YAG laser at 1.06 μm. The pump beam was mode matched to the cavity with a single 100-mm focal length lens. As much as 17-W pump power was available.

B. Periodically Poled Lithium Niobate Crystals

The OPO PPLN crystal in this experiment had an aperture of 0.5 mm × 10 mm, a length of 50 mm, and a domain period of $\Lambda_1 = 30.5$ μm for quasi-phase matching. The OPO process can produce a resonant cw signal between 1.70 and 1.73 μm and an idler between 2.84 and 2.77 μm from the 1.06-μm pump over the crystal temperature range of 170–190 °C. Both input and output surfaces of the crystal were antireflection coated for the pump ($R < 1\%$), signal ($R < 0.1\%$), and idler ($R < 5\%$) wavelength regions. Two DFG PPLN crystals, 30 and 50 mm in length and 1 mm × 10 mm in cross section, were tested in the OPO resonator. The thicker PPLN used for DFG crystals was to reduce additional insertion losses for the OPO signal and idler in the resonator. The DFG crystals had eight grating bands with domain periods (Λ_2) of 29.5, 29.7, 29.9, 30, 30.2, 30.4, 30.6, and 30.8 μm to phase match the OPO signal and idler waves to generate a MWIR output (4–5-μm). Thus, tunable MWIR output (4–5 μm) was produced by adjustment of the temperature of the OPO and DFG crystals, and selection of the appropriate DFG grating period to allow proper phase matching of the OPO signal, idler, and MWIR waves. The DFG crystal surfaces were broadband antireflection coated to minimize reflectivity ($R < 0.1\%$) at the OPO signal wavelengths, whereas $R < 2\%$ at idler wavelengths and $R < 10\%$ at MWIR wavelengths. Both OPO and DFG crystals were mounted in separate ovens, allowing for independent temperature control from room temperature to 200 °C with an accuracy of ±0.2 °C.

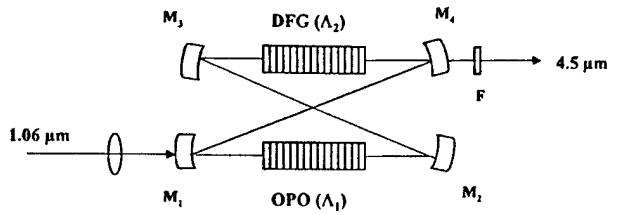

Fig. 1. Optical schematic of the cw tunable MWIR OPO DFG resonator device.

4. EXPERIMENTAL RESULTS WITH DIFFERENCE FREQUENCY GENERATION

A. Wavelength Tuning

By use of this OPO DFG device, a tunable MWIR wavelength from 4.25 to 4.65 μm was demonstrated. Figure 2 shows the experimental DFG output wavelength versus phase-matching temperature obtained for all eight grating bands (29.5–30.8 μm) of the DFG crystal. I obtained each data point in Fig. 2 by first selecting the DFG grating period, setting the DFG crystal temperature, and then tuning the OPO crystal temperature until the MWIR signal was maximized. The Nd:YAG laser provides temperature-tuned signal (1702–1732-nm) and idler (2840–2760-nm) wavelengths. For the measurements, the actual MWIR wavelength was calculated from the OPO signal and idler wavelengths that were directly measured with a Burleigh WA-1500IR wavemeter. (The wavemeter could not be used to measure wavelengths beyond 4 μm). The 0.05-nm accuracy of the wavemeter in the OPO wavelength region allows the MWIR wavelengths to be calculated to within ±0.7 nm. In Fig. 2, the theoretical calculations are shown as dashed curves. These curves were generated first by selection of the DFG period Λ_2 and the crystal temperature. Then pairs of wavelengths that satisfy the OPO [Eq. (2)] and the DFG [Eqs. (4) and (5)] were used to generate the DFG wavelengths. The temperature-dependent refractive index was calculated from the Sellmeier equation of Ref. 10. Some discrepancies between the experimental and the calculated curves are obvious and are discussed in Subsection 5.A.

B. Output Power Performance

Power output at 4.5-μm versus 1.06-μm pump power was measured for the 30- and 50-mm PPLN DFG crystals. The results, shown in Fig. 3, were obtained by use of the 30-μm DFG grating band and a crystal temperature of 100 °C. The OPO PPLN temperature was set at 183 °C to produce the required signal and idler wavelengths of 1.721 and 2.788 μm. For the 50-mm crystal, 90 mW in the MWIR was achieved for a pump power of 16.7 W. The 2.788-μm idler power was measured to be 2.5 W. Under the same pumping conditions, only 40 mW of MWIR power was obtained from the 30-mm crystal. The cavity resonator length was adjusted for both measurements to ensure that comparable spot sizes were obtained within the two DFG crystals. It was further noted that, for fixed pump powers, the OPO idler power would slightly increase as the DFG output was optimized because of amplification of the idler by the DFG process.

C. Spectral Bandwidth Measurement

The MWIR output spectrum was also measured with a scanning Jobin Yvon ISA 550 IR spectrometer with

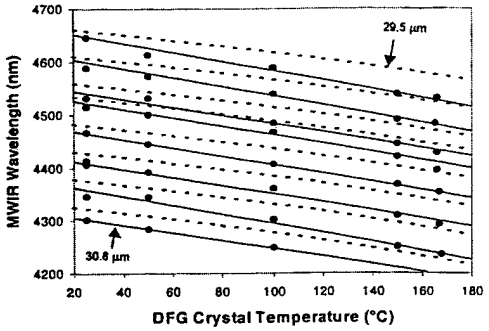

Fig. 2. MWIR wavelength tuning versus temperature for each DFG PPLN grating period. The filled circles and the solid lines denote the experimental data and curve fits for each of the eight DFG grating bands (see Subsection 3.B) that range from 29.5 μm (top) to 30.8 μm (bottom). The dashed curves were calculated with the Sellmeier equation of Ref. 10 for the same grating periods.

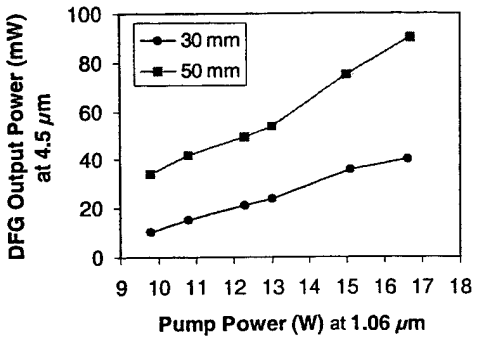

Fig. 3. MWIR output power performances for the 30- and 50-mm DFG crystal at 4.5 μm versus 1.06-μm pump power.

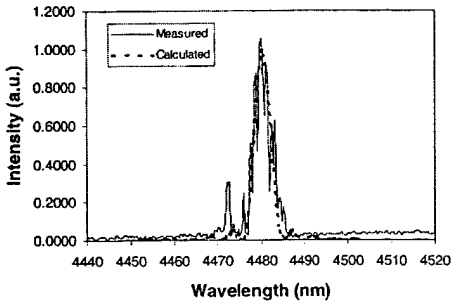

Fig. 4. MWIR spectral profile measured by the IR spectrometer. The solid curve is the theoretical DFG spectral profile calculated with the Sellmeier equation given in Ref. 10 at 100 °C for a 30-μm PPLN grating. The calculated peak was shifted to match the data.

0.2-nm resolution. A sample spectrum taken at 100 °C (the same condition as described in subsection 3.B for the 50-mm DFG PPLN) is shown in Fig. 4. Wavelength fluctuations (noise) in the OPO signal, measured to be of the order of 1.1 nm, should result in a MWIR spectral width of the order of 15 nm. The actual measured linewidth, however, is only ~4.5 nm (FWHM), which is most likely indicative of the DFG spectral acceptance bandwidth. A comparison with the theoretical bandwidth is discussed in Subsection 5.B.

5. DISCUSSION OF DIFFERENCE FREQUENCY GENERATION

A. Wavelength Tuning

The calculated wavelength versus temperature curves shown in Fig. 2 consistently yield longer MWIR wavelengths than the measurements. Furthermore, the difference between theory and experiment increases with temperature. As an example, the calculated DFG wavelength at 100 °C for the 30-μm grating period is approximately 20 nm longer than the measured value, whereas the difference at 160 °C is approximately 35 nm. The discrepancy between theory and data can be attributed to inaccuracies of the Sellmeier equation as presented in Ref. 10 and to MWIR absorption by the crystal that possibly increases the temperature along the beam path beyond the value given by the crystal temperature controller.

B. Spectral Acceptance Bandwidth

The DFG acceptance bandwidth can be determined from the DFG spectral profile. Experimental and calculated spectra for $\Lambda_2 = 30$ μm, T = 100 °C, and a crystal length of 50 mm are shown in Fig. 4. The calculated profile is derived from a DFG parametric gain expression, such as that given in Ref. 9. The ratio of the phase-mismatched DFG intensity $I(\Delta k_{DFG})$ to the phase-matched (peak) intensity $I(0)$ can be expressed as

$$I(\Delta k_{DFG})/I(0) = \mathrm{sinc}^2(\Delta k_{DFG} L/2), \qquad (6)$$

where $\Delta k_{DFG} = n_s/\lambda_s - n_i/\lambda_i - n_{MWIR}/\lambda_{MWIR} - 1/\Lambda_2$. The calculated profile was determined from $\lambda_s\lambda_i$ pairs obtained from Eq. (2) and refractive index n derived from the Sellmeier equation given in Ref. 10. Because of the inability of this equation to yield the refractive index in our test region accurately, the calculated peak needed to be shifted in wavelength so that it would coincide with the experimental data. The equation, however, was reasonably accurate in predicting an acceptance bandwidth. The calculation yielded a 4.2-nm acceptance bandwidth for the DFG process. The measured spectral profile agrees well with the calculations, as can be seen in Fig. 4. The DFG spectral acceptance bandwidth of 4.2 nm can be calculated directly from Eq. (6) for $I(\Delta k_{DFG})/I(0) = 0.5$, i.e., $\Delta k_{DFG} L/2 = 1.39$.[9] The conditions and calculated results are listed in Table 1. This excellent agreement between the theory and the experimental measurement confirmed that the measured spectral bandwidth of 4.5 nm is the DFG acceptance bandwidth. The only noticeable discrepancy between the theory and the observation is the appearance of a rather strong repeatable peak at 4472 nm near the wavelength at which theory would predict the first maximum to occur [see Eq. (6)]. Furthermore, a corresponding maximum on the longer wavelength side was not observed. Reasons for this are still unknown.

C. Power Conversion

Figure 3 shows that DFG power conversion for the 50-mm crystal is significantly higher than for the 30-mm crystal. An analysis was performed based on the DFG power equation given by Ref. 11. Since all the parameters in this equation are basically the same, the DFG power is simply proportional to crystal length L and the focusing

Table 1. Calculated Phase-Matching Wavelengths and Acceptance Bandwidths for DFG in a 30-μm Grating Period PPLN at 100 °C

Phase-Matching Waves for DFG	$\Delta k_Q L/2$ = 0[b]	$\Delta k_Q L/2$ = 1.39[c]	$\Delta k_Q L/2$ = −1.39[c]	Acceptance Bandwidths[d]
OPO signal wave[a] (nm)	1720.3	1720.4	1720.1	0.3
OPO idler wave[a] (nm)	2788.9	2788.5	2789.3	0.8
MWIR (nm)	4489.8	4491.9	4487.7	4.2

[a] OPO wavelengths generated with a 1064-nm fixed-wavelength pump laser.
[b] Phase-matched condition at 100 °C.
[c] Half-maximum for the DFG parametric gain (wavelength tolerance) for a 50-mm DFG PPLN at 100 °C.
[d] Wavelength differences between column 3 and 4 give acceptance bandwidth (FWHM) of DFG waves at 100 °C for a 5-cm PPLN.

function $h(\mu, \xi)$. In this function, μ is the ratio of the input wave vectors ($k_s/k_i = 0.62$), and ξ is the ratio of the crystal length to the confocal parameter. For this experimental condition, the focusing parameter for the longer crystal is estimated to be larger than that of the shorter crystal by a factor of approximately 1.2. Therefore, when the focusing parameter and the length are considered, the 50-mm DFG crystal should have a power conversion that is twice as large as the 30-mm crystal, which is close to that observed. Other factors that need to be considered include optical coating loss, aperture loss, and optical absorption by the crystal.

D. Output Stability

The MWIR power fluctuations observed in Fig. 4 are due to mode hopping of the OPO signal in the resonant cavity during the spectral scan. This mode hopping is most likely related to the photorefractive effect in lithium niobate, which has been discussed in recent publications.[2,12–14] As discussed in Ref. 2, the photorefractive effect is typically seen in an IR OPO experiment with high-power pumping. The cause of the damage is not the pump beam itself but second-harmonic generation green light from the pump, which results from a higher-order doubling process. The photorefractive effect is known to cause distortion in the beam profile.[15] In the DFG experiments discussed here, intermittent distortion of the green light coincided with the occurrence of mode hopping and power fluctuations in the OPO operation. This suggests that mode hopping is caused by the photorefractive effect. Not only do the OPO wavelength fluctuations translate into MWIR amplitude noise, but the wavelength instability is also more severe in our case because of the limited DFG acceptance bandwidth. Reducing the wavelength fluctuations should reduce the DFG noise and also increase the average power by keeping the OPO wavelengths within the PPLN acceptance bandwidth. Recently tested magnesium oxide-doped PPLN has been shown to be more resistant to this effect than nondoped PPLN for waveguide devices.[14] Using magnesium oxide-doped PPLN could be the solution to suppress the MWIR fluctuations observed in this OPO DFG device. Other materials that do not exhibit the photorefractive effect, such as periodically poled $RbTiOAsO_4$,[16,17] could also be an alternative for low-noise operation.

6. CONCLUSION

In conclusion, tunable cw MWIR in the 4.25–4.65-μm spectral range was demonstrated by use of a two-PPLN crystal OPO DFG device. A maximum power of 90 mW was achieved at 4.5 μm. The measured MWIR spectral bandwidth of 4.5 nm (FWHM) agrees quite well with the theoretical value of 4.2 nm. The OPO DFG device can extend to even longer wavelengths with the proper choice of DFG PPLN coatings and appropriate (smaller) grating periods. The MWIR output power stability and average power could be greatly improved if the magnesium oxide-doped PPLN or other materials without a photorefractive effect were used to reduce the OPO wavelength fluctuations.

ACKNOWLEDGMENT

The author thanks Henry Montes, Todd S. Rose, and Frank L. Vernon, Jr., of the Aerospace Corporation for providing valuable technical support. This research was supported by U.S. Air Force contract FO4701-00-C-0009.
Da-Wun Chen's e-mail address is dawun.chen@aero.org.

REFERENCES

1. W. R. Bosenberg, A. Drobshoff, J. I. Alexander, L. E. Myers, and R. L. Byer, "93% pump depletion, 3.5-W continuous-wave, singly resonant optical parametric oscillator," Opt. Lett. **21**, 1336–1338 (1996).
2. L. E. Myers and W. R. Bosenberg, "Periodically poled lithium niobate and quasi-phase-matched optical parametric oscillators," IEEE J. Quantum Electron. **33**, 1663–1671 (1997).
3. L. E. Myers, R. C. Eckardt, M. M. Fejer, R. L. Byer, and W. R. Bosenberg, "Multigrating quasi-phase-matched optical parametric oscillator in periodically poled $LiNbO_3$," Opt. Lett. **21**, 591–593 (1996).
4. M. Brown, A. J. W. Brown, C. Miyake, F. Futtere, and D. Smith, "A 10 kHz PPLN OPO operating in a region of very high idler absorption," in *Advanced Solid-State Lasers*, M. M. Fejer, H. Injeyan, and U. Keller, eds., Vol. 26 of OSA Trends in Optics and Photonics Series (Optical Society of America, Washington, D.C., 1999), pp. 554–557.
5. D. J. M. Stothard, M. Ebrahimzadeh, and M. H. Dunn, "Low-pump-threshold continuous-wave singly resonant optical parametric oscillator," Opt. Lett. **23**, 1895–1897 (1998).
6. L. Goldberg, W. K. Burns, and R. W. McElhanon, "Difference-frequency generation of tunable mid-infrared radiation in bulk periodically poled $LiNbO_3$," Opt. Lett. **20**, 1280–1282 (1995).
7. P. Loza-Alvarez, C. T. A. Brown, D. T. Reid, W. Sibbett, and M. Missey, "High-repetition-rate ultrashort-pulse optical parametric oscillator continuously tunable from 2.8 to 6.8 μm," Opt. Lett. **24**, 1523–1525 (1999).
8. D. Chen and K. Masters, "Continuous-wave 4.3-μm intracavity difference frequency generation in an optical parametric oscillator," Opt. Lett. **26**, 25–27 (2001).
9. L. E. Myers, R. C. Eckardt, M. M. Fejer, R. L. Byer, W. R. Bosenberg, and J. W. Pierce, "Quasi-phase-matched optical parametric oscillators in bulk periodically poled $LiNbO_3$," J. Opt. Soc. Am. B **12**, 2102–2116 (1995).
10. D. H. Jundt, "Temperature-dependent Sellmeier equation

for the index of refraction, n_e, in congruent lithium niobate," Opt. Lett. **22**, 1553–1555 (1997).
11. P. Canarelli, Z. Bendo, R. Curl, and E. K. Tittel, "Continuous-wave infrared laser spectrometer based on difference frequency generation in $AgGaS_2$ for high-resolution spectroscopy," J. Opt. Soc. Am. B **9**, 197–202 (1992).
12. W. R. Bosenberg, J. I. Alexander, L. E. Myers, and R. W. Wallace, "2.5-W, continuous-wave, 629-nm solid-state laser source," Opt. Lett. **23**, 207–209 (1998).
13. C. Q. Xu, H. Okayama, and Y. Ogawa, "Photorefractive damage of $LiNbO_3$ quasiphase matched wavelength converters," J. Appl. Phys. **87**, 3203–3208 (2000).
14. R. G. Batchko, R. Roussev, and M. H. Sher, "All-optical MgO:$LiNbO_3$ wavelength converter for telecommunications," in *Advanced Solid State Lasers*, Vol. 68 of OSA Trends in Optics and Photonics Series (Optical Society of America, Washington, D.C., 2002), Post deadline paper PD5.
15. V. Pruneri, J. Webjörn, P. St. J. Russell, and D. C. Hanna, "532 nm pumped optical parametric oscillator in bulk periodically poled lithium niobate," Appl. Phys. Lett. **67**, 2126–2128 (1995).
16. T. J. Edwards, G. A. Turnbull, M. H. Dunn, M. Ebrahimzadeh, H. Karlsson, G. Arvidsson, and F. Laurell, "Continuous-wave singly resonant optical parametric oscillator based on periodically poled $RbTiOAsO_4$," Opt. Lett. **23**, 837–839 (1998).
17. H. Karlsson, M. Olson, G. Arvidsson, F. Laurell, U. Bäder, A. Borsutzky, R. Wallenstein, S. Wickström, and M. Gustafsson, "Nanosecond optical parametric oscillator based on large-aperture periodically poled $RbTiOAsO_4$," Opt. Lett. **24**, 330–332 (1999).

LABORATORY OPERATIONS

The Aerospace Corporation functions as an "architect-engineer" for national security programs, specializing in advanced military space systems. The Corporation's Laboratory Operations supports the effective and timely development and operation of national security systems through scientific research and the application of advanced technology. Vital to the success of the Corporation is the technical staff's wide-ranging expertise and its ability to stay abreast of new technological developments and program support issues associated with rapidly evolving space systems. Contributing capabilities are provided by these individual organizations:

Electronics and Photonics Laboratory: Microelectronics, VLSI reliability, failure analysis, solid-state device physics, compound semiconductors, radiation effects, infrared and CCD detector devices, data storage and display technologies; lasers and electro-optics, solid-state laser design, micro-optics, optical communications, and fiber-optic sensors; atomic frequency standards, applied laser spectroscopy, laser chemistry, atmospheric propagation and beam control, LIDAR/LADAR remote sensing; solar cell and array testing and evaluation, battery electrochemistry, battery testing and evaluation.

Space Materials Laboratory: Evaluation and characterizations of new materials and processing techniques: metals, alloys, ceramics, polymers, thin films, and composites; development of advanced deposition processes; nondestructive evaluation, component failure analysis and reliability; structural mechanics, fracture mechanics, and stress corrosion; analysis and evaluation of materials at cryogenic and elevated temperatures; launch vehicle fluid mechanics, heat transfer and flight dynamics; aerothermodynamics; chemical and electric propulsion; environmental chemistry; combustion processes; space environment effects on materials, hardening and vulnerability assessment; contamination, thermal and structural control; lubrication and surface phenomena. Microelectromechanical systems (MEMS) for space applications; laser micromachining; laser-surface physical and chemical interactions; micropropulsion; micro- and nanosatellite mission analysis; intelligent microinstruments for monitoring space and launch system environments.

Space Science Applications Laboratory: Magnetospheric, auroral and cosmic-ray physics, wave-particle interactions, magnetospheric plasma waves; atmospheric and ionospheric physics, density and composition of the upper atmosphere, remote sensing using atmospheric radiation; solar physics, infrared astronomy, infrared signature analysis; infrared surveillance, imaging and remote sensing; multispectral and hyperspectral sensor development; data analysis and algorithm development; applications of multispectral and hyperspectral imagery to defense, civil space, commercial, and environmental missions; effects of solar activity, magnetic storms and nuclear explosions on the Earth's atmosphere, ionosphere and magnetosphere; effects of electromagnetic and particulate radiations on space systems; space instrumentation, design, fabrication and test; environmental chemistry, trace detection; atmospheric chemical reactions, atmospheric optics, light scattering, state-specific chemical reactions, and radiative signatures of missile plumes.